

Multiscale Cloud-based Pipeline for Neuronal Electrophysiology Analysis and Visualization

Jinghui Geng  ^{1,4,*}, Kateryna Voitiuk  ^{1,2,4}, David F. Parks  ^{2,4}, Ash Robbins  ^{1,4}, Alex Spaeth  ^{1,4}, Jessica L. Sevetson  ^{3,4}, Sebastian Hernandez ^{1,4}, Hunter E. Schweiger  ^{3,4}, John P. Andrews  ⁵, Spencer T. Seiler  ^{1,2,4}, Matthew A.T. Elliott  ^{2,4}, Edward F. Chang ^{5,6}, Tomasz J. Nowakowski  ^{5,6,7,8,9}, Rob Currie ⁴, Mohammed A. Mostajo-Radji  ⁴, David Haussler  ^{2,4}, Tal Sharf  ^{2,4}, Sofie R. Salama  ^{3,4}, Mircea Teodorescu  ^{1,2,4,*}

¹Department of Electrical and Computer Engineering, University of California Santa Cruz, Santa Cruz, CA, USA

²Department of Biomolecular Engineering, University of California Santa Cruz, Santa Cruz, CA, USA

³Department of Molecular, Cell, and Developmental Biology, University of California Santa Cruz, Santa Cruz, CA, USA

⁴Genomics Institute, University of California Santa Cruz, Santa Cruz, CA, USA

⁵Department of Neurological Surgery, University of California San Francisco, San Francisco, CA, USA

⁶Weill Institute for Neurosciences, University of California San Francisco, San Francisco, CA, USA

⁷The Eli and Edythe Broad Center of Regeneration Medicine and Stem Cell Research, University of California San Francisco, San Francisco, CA, USA

⁸Department of Psychiatry and Behavioral Sciences, University of California San Francisco, San Francisco, CA, USA

⁹Department of Anatomy, University of California San Francisco, San Francisco, CA, USA

*Correspondence Author. Email: jgeng2@ucsc.edu, mteodorescu@ucsc.edu

ABSTRACT

1 **Electrophysiology offers a high-resolution method for real-time measurement of neural
2 activity. The vast amount of data generated requires efficient storage and sophisticated
3 processing to extract neural function and network dynamics. However, analysis is of-
4 ten challenging due to the need for multiple software tools with different runtime depen-
5 dencies. Longitudinal recordings from high-density microelectrode arrays (HD-MEAs)
6 can be of considerable size for local storage, complicating data management, sharing,
7 and backup. To address these challenges, we developed an open-source cloud-based
8 pipeline to store, analyze, and visualize neuronal electrophysiology recordings from HD-
9 MEAs. This pipeline is dependency agnostic by utilizing cloud storage, cloud computing
10 resources, and an Internet of Things messaging protocol. We containerized the analy-
11 sis algorithms to serve as scalable and flexible building blocks within the pipeline. We
12 designed graphical user interfaces and command line tools to remove the requirement
13 of programming skills. The interactive visualizations provide multi-modality information
14 on various neuronal features. This cloud-based pipeline is an efficient solution for elec-
15 trophysiology data processing, the limitations of local software tools, and storage con-
16 straints. It simplifies the electrophysiology data analysis process and facilitates under-
17 standing neuronal activity. In this paper, we applied this pipeline on two types of cultures,
18 cortical organoids and *ex vivo* brain slice recordings.**

19 INTRODUCTION

20 Recent advances in hardware and software platforms for neuronal recordings have enabled si-
21 multaneous recording of neuronal activity with high spatial and temporal resolution across var-

22 ious samples, including brain slices¹², 2D cultures³⁻⁵, and 3D cerebral organoids⁶⁻⁷. These
23 technologies facilitate comprehensive studies of brain function, neurodevelopment, and network
24 topology⁸⁻¹⁰. However, the exponential growth in data volume and complexity¹¹⁻¹³ presents sig-
25 nificant challenges in data storage, processing, and analysis. Recordings, images, and analysis
26 results can consume substantial storage on computers and hard drives. Interpreting this multi-
27 dimensional data requires specialized algorithms and tools to extract single neuronal unit activity,
28 visualize firing patterns, and understand neuronal network-level information¹⁴⁻¹⁶. While efforts
29 have been made to unify standards in electrophysiology, biologists still face difficulties performing
30 comprehensive analyses.

31 Spike sorting algorithms are crucial for analyzing multi-electrode array (MEA) recordings¹⁷⁻²¹,
32 identifying and categorizing individual neuronal spikes from raw voltage traces to analyze neu-
33 ronal features²²⁻²⁵ and network dynamics²⁶⁻²⁷. While various software tools have been devel-
34 oped to process MEA recordings and visualize neuronal features²³⁻²⁸⁻³³, challenges persist due
35 to differing programming languages, limited user support, and compatibility issues. Although in-
36 tegrated platforms offer end-to-end analysis capabilities, they may restrict custom data manipula-
37 tion, requiring researchers to develop their own workflows and navigate steep learning curves for
38 effective data interpretation.

39 Cloud computing enables processing a large amount of data in parallel by utilizing abundant re-
40 sources while still being a cost-effective solution³⁴⁻³⁶. Cloud-based storage can address the is-
41 sue of massive experimental data filling up local disks. It also provides extensive data sharing
42 ability for collaborations across research labs. Infrastructures and web platforms have been de-
43 veloped to store and analyze various types of data, including electrophysiology, neuroimaging,
44 and sequencing³⁷⁻⁴². These platforms are designed to benefit the broader neuroscience com-
45 munity, emphasizing data publication and sharing⁴³⁻⁴⁴. A research laboratory-oriented data plat-
46 form is needed to support consistent experiments and data processing.

47 The Internet of Things (IoT) has made a significant impact in many fields, including healthcare⁴⁵⁻⁴⁶
48 and, in recent years, has been applied to cellular biology⁴⁷⁻⁴⁸ and in vitro electrophysiology ex-
49 periments⁴⁹⁻⁵¹. Its resource efficiency enables the messaging protocol to work across different
50 hardware, allowing networks to grow from a few devices to a large number without compromising
51 performance.

52 We developed a cloud-based pipeline for electrophysiology data storage, processing, and shar-
53 ing to facilitate the day-to-day research. We used containerization as the minimum building block.
54 The IoT messaging services and data analysis algorithms are packaged into individual contain-
55 ers. The IoT services run on a web server to stream data, monitor processing tasks, and com-
56 municate with researchers through user interfaces. We applied Kubernetes⁵² to orchestrate the
57 analysis containers on the cloud computing clusters. By using cloud computing resources, the
58 pipeline can process a large number of datasets with different algorithms in parallel, optimizing
59 resource utilization, scalability, and flexibility. Moreover, we lower costs by replacing local com-
60 puting hardware, such as CPUs and GPUs, with cloud-based technology. We also remove the
61 barriers to data analysis by providing user interfaces, minimizing the software setup process,
62 and making the Python code open source. The pipeline provides a suite of algorithms, includ-
63 ing spike sorting, autocuration of putative neural units, visualization, and downstream analyses
64 for specific goals using the curated data. We tested this pipeline with two applications. First, we
65 analyzed mouse cortical organoid longitudinal recordings, 10 minutes long, one hour apart, over
66 a 7-day period. This demonstrated the utility of our approach for neuron tracking. Second, we ap-
67 plied the pipeline to study optogenetic modulation of epileptiform activity in human hippocampus
68 slices, contributing to our understanding and potential treatment of neurological diseases.

69 RESULTS

70 Our platform allows users to upload recordings from electrophysiology devices directly to cloud
71 storage. The data is organized by experiment date and is annotated with automatically extracted
72 as well as user-specified metadata. The pipeline can be scaled up as algorithms and services
73 are containerized, making it easy to integrate new analytical tools as they become available. The
74 pipeline supports multiple data processing paradigms to accommodate diverse research require-
75 ments. The graphical interface allows users to initiate, monitor, and visualize data processing
76 after upload, offering multimodal analysis and result downloads. An integrated IoT messaging
77 service connects users, local recording devices, and the cloud, streamlining workflow.

78 Framework Design

79 The pipeline is generic and capable of processing data from any electrophysiology platform that
80 uses HDF5 and NWB⁵³⁻⁵⁵ formats. In this paper, we tested it with data generated by a MaxOne
81 HD-MEA (MaxWell Biosystems)⁵⁶. The system has 26,400 electrodes in a 2.10x3.85mm² area.
82 It supports data collection from 1,020 channels and can simulate 32 channels simultaneously at
83 a 20kHz sample rate. Together with a small inter-electrode pitch (17.5μm), the system provides
84 high temporal and spatial resolution, where the activity of a typical neuron will be recorded on
85 multiple pads. We utilize Ceph S3 and the National Research Platform (NRP) computing clusters
86 for data storage and processing.

87 The overview of the platform is shown in Figure 1. Neuronal tissue culture activity data is col-
88 lected on a MaxWell MEA headstage, connected to a local computer running MaxLab software
89 (Figure 1A). After recording, datasets are streamed to S3 and the data uploader generates cor-
90 responding metadata and maintains the applicable S3 file structure for these datasets (Figure
91 1B). Upon completion, an MQTT message is sent from the data uploader to the processing ser-
92 vice – the job listener. This message contains the experiment identifiers and the image of the
93 dockerized algorithm. The listener parses the message to gather the S3 paths for each dataset
94 and calls the Kubernetes-Python API to deploy data processing jobs to the NRP computing clus-
95 ter 15. The pipeline provides several containerized data processing applications, including spike
96 sorting, data curation, and visualization. Once a job is completed on the NRP, the result is saved
97 to S3 (Figure 1C). Researchers can access and download these results through the user inter-
98 face.

99 To make the pipeline accessible to non-programmers, we have developed user interfaces for
100 managing and interacting with both local and remote data processes (Figure 2A). Through these
101 interfaces, researchers can have complete control over their data while bridging the gap between
102 running complex algorithms and requiring extensive programming knowledge or technical exper-
103 tise.

104 These interfaces include a data uploader, a Dashboard webpage, and a Slack channel, each
105 serving distinct purposes while bridging local data collection, cloud-based data manipulation,
106 and user notifications. The data uploader, installable on local laptops, enables users to upload
107 electrophysiology recordings to S3 storage and initiate batch processing jobs with predefined
108 parameters after the experiment is finished. The web Dashboard, accessible from any internet-
109 connected device, provides access to existing S3 data for both batch and chained jobs. The data
110 uploader and the Dashboard support downloading files from S3 to local directories. Addition-
111 ally, the Dashboard features a visualization page displaying post-processing figures of selected
112 recordings. A Slack channel is used to post status notifications for data processing jobs. Detailed
113 descriptions of these user interfaces are provided in the Methods section. Screenshots of the ap-
114 plications are shown in Supplementary Figure S2, S3.

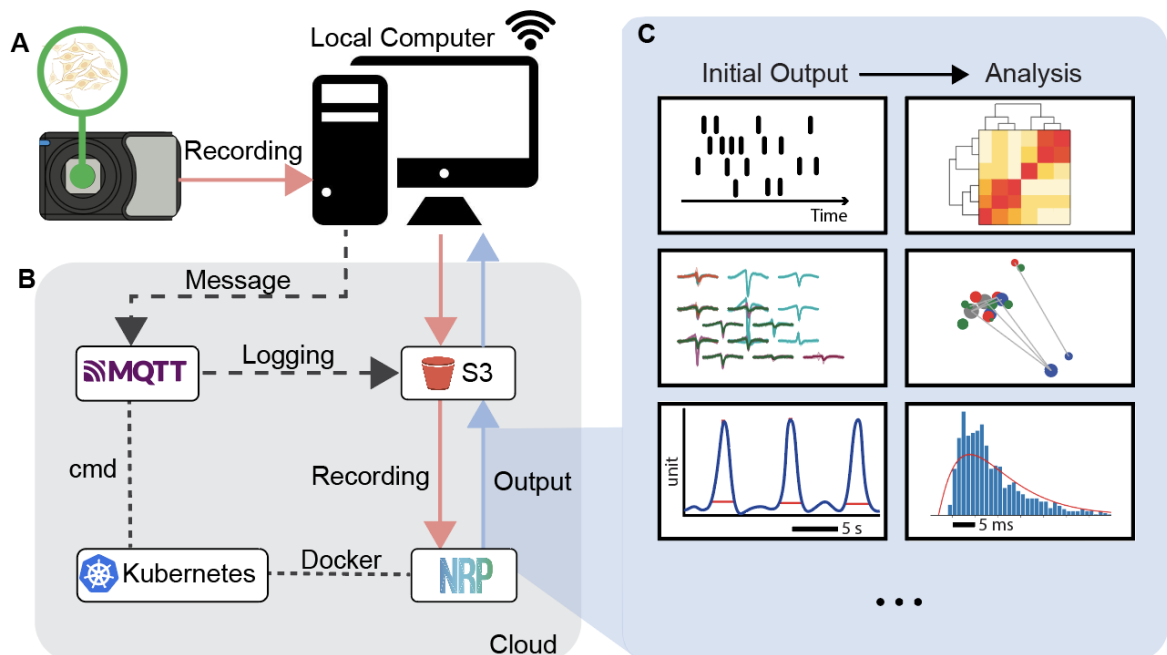


Figure 1: Cloud-based electrophysiology data processing pipeline architecture. (A) Electrophysiology data from neuronal cultures is recorded on a local computer. Different neuronal cultures and their recordings are shown in Figures 4 and 7. (B) Once the dataset is saved, it is uploaded to a uniquely identified data bucket AWS S3 for permanent storage using the Uploader. An MQTT message is simultaneously sent to the job listener service to initiate data processing jobs. These jobs run containerized algorithms and are launched on the National Research Platform (NRP) computing cluster using Kubernetes. Results, including post-processed data and figures, are saved back to AWS S3. (C) The analysis outputs various interactive analytical figures for each dataset's network features and single-unit activity.

115 For cloud integration, we used the Message Queuing Telemetry Transport (MQTT) messaging
116 protocol, a lightweight publish-subscribe protocol designed for Internet-of-Things (IoT) appli-
117 cations. This approach reduces the dependency requirements for edge devices to run cloud-
118 computing jobs. A local computer can utilize the pipeline as long as it can run a Python envi-
119 ronment and has a network connection. We have designed job listener and scanner services to
120 run and monitor jobs on the cloud (Figure 2B,C). For cloud computing, we used the National Re-
121 search Platform (NRP), a distributed commodity compute cluster based on Kubernetes and the
122 Ceph distributed file system. It has special CPUs and GPUs for data science, simulations, and
123 machine learning. This setup allows for parallel data processing and can help reduce the com-
124 puting infrastructure cost of individual labs.

125 We have a job scanner (Figure 2B) that checks on data processing jobs in the cloud every 30
126 minutes. It updates a list of current job statuses using the Kubernetes Python API. The scanner
127 reads job names and information, which are named based on the dataset or a job list. This helps
128 the scanner find the correct information in the NRP. The scanner then updates the listener and
129 the user about how jobs are progressing.

130 To keep the flexibility of data processing, we implemented two types of jobs: batch processing
131 and chained jobs. Chained jobs run through several steps on different data, with subsequent
132 processing dependent on prior results. When the scanner detects a status change in a chained
133 job, it sends a message to the listener to update the corresponding job look-up table and initiate
134 the next processing step. Concurrently, it notifies the user about completing the prior job and the
135 start of the next. This notification is done through the “slack-bridge” service. For completed batch
136 processing jobs, the scanner sends only a user notification. After a message is sent, finished
137 jobs are removed from the scanner’s memory to prevent duplicate notifications.

138 The job listener (Figure 2C) receives messages from both the user interface and the scanner. It
139 also sends user notifications to the “ephys-pipeline” Slack channel. The primary function of the
140 job listener is to initiate cloud computing jobs. Upon receiving a run job message, the listener
141 parses it to extract the data path, data format, parameter setting, and job type (analysis algo-
142 rithms). The listener then calls functions from a Python Kubernetes object (Figure 2) to allocate
143 computing resources on NRP and the appropriate analysis docker image for each dataset. This
144 object creates a job on the NRP and a pod within each job. Finally, it sends a “job created” no-
145 tification to the Slack channel. Both the scanner and listener services maintain logs on S3 for
146 historical tracking and ease of maintenance. These logs are updated after each new message is
147 received or sent.

148 The data organization on S3 (Figure 2D) is structured based on data types and characteristics.
149 Electrophysiology recordings are grouped by experiment batch, assigned a universally unique
150 identifier (UUID), and paired with a “metadata.json” file for overall content description and ex-
151 periment notes. We create sub-buckets: “original/data” for raw recordings and “derived/algo” for
152 analysis output, where “algo” represents the algorithm used to analyze the data. Additionally, we
153 maintain a “service” bucket for the chained job scheduler and logging of listener and scanner ac-
154 tivities. Since the computing clusters are designed to run containerized data processing jobs, we
155 have created docker images for electrophysiology algorithms with minimum software dependen-
156 cies.

157 As illustrated in Figure 2E, when the listener deploys a job to NRP, the platform assigns a node
158 with all the requested resources. The node creates a pod, pulls the docker image from Docker-
159 Hub, and retrieves data from S3 to run the analysis. The processing results are then uploaded
160 back to S3 from the container. Figure 2F demonstrates an example of a containerized batch pro-

161 cessing algorithm. In this container, a Python script reads an electrophysiology recording, per-
162 forms spike sorting on the raw data to identify putative firing neurons (single units), applies au-
163 tocuration to preserve high-quality units, and generates both visualization figures and spike data
164 for the recording. The spike data is stored as a NumPy data structure with temporal and spatial
165 information of the single units.

166 Figure 2G shows the Python Kubernetes object configuration in the listener for job execution.
167 This configuration specifies the number of CPUs and GPUs and the amount of memory and stor-
168 age required to run a specific container. These resource allocations are calculated based on the
169 algorithm workload and data size, optimized for efficient utilization of cloud computing resources.
170 To execute a specific container, the configuration is provided with the corresponding docker im-
171 age, input data (such as the recording or derived results from the recording), and metadata (in-
172 cluding data format or parameter settings). Examples of Kubernetes configurations can be found
173 in Supplementary Table S2.

174 **This Pipeline Enables Versatile Jobs**

175 Data processing and analysis often require multiple iterations for new experiments due to changes
176 in recording hardware, biological samples, and data requirements. To ensure versatility in data
177 processing jobs, we developed a minimum building block for the pipeline and designed various
178 job execution paradigms.

179 Figure 3A shows the minimum building blocks of our pipeline. It includes paths to S3 data stor-
180 age and a containerized algorithm. Each algorithm needs two inputs (data and parameters) and
181 produces one output file with results (processed data, visualization figures, and logs). We store
182 input data and outputs in designated buckets on S3 under each UUID. We keep these param-
183 eters in designated sub-buckets (“service/params/algo”) on S3, named after each algorithm.
184 Users can pick existing parameters or make new ones on the Dashboard’s “Job Center” page
185 (Figure 3B, Supplementary Figure S3).

186 The pipeline supports both batch processing and chained jobs (Figure 3C,D). Batch processing
187 enables the analysis of numerous recordings using identical parameter settings. All jobs can be
188 processed in parallel on NRP. Users can initiate a batch job from the local data uploader after
189 the experiment. In batch processing, each recording undergoes spike sorting, autocuration, and
190 visualization. Detailed descriptions of these three steps can be found in the Methods section.

191 As algorithms are packaged in individual docker containers as minimum building blocks, multiple
192 analysis jobs can be chained for a recording, with stage results passed to subsequent jobs upon
193 completion of the previous job (Figure 3D). To implement this functionality, we designed a CSV
194 job scheduler integrated into the Dashboard, Listener, and Scanner services. When users se-
195 lect recordings and a list of analysis jobs from the Dashboard, a CSV file is generated, with each
196 row representing an analysis job. Columns contain sufficient information to initiate the job, includ-
197 ing the S3 data path, computing resource requirements (job metadata), and parameter settings.
198 We use the “next_job” column to index the row of the job to run after the current row, allowing for
199 multiple indices. After saving this CSV file to S3, the Dashboard sends a message to the Listener
200 to start the first stage jobs by indexing them in the message body. We create the NRP job name
201 using the CSV file name, enabling the Scanner to differentiate chained jobs from batch jobs by
202 simply parsing the name. Upon completing the first stage jobs, the Scanner sends the Listener
203 an “update” message. The Listener then checks for any available “next_job” in the CSV file and
204 launches the second-stage jobs. Detailed information on job chaining can be found in the Meth-
205 ods section.

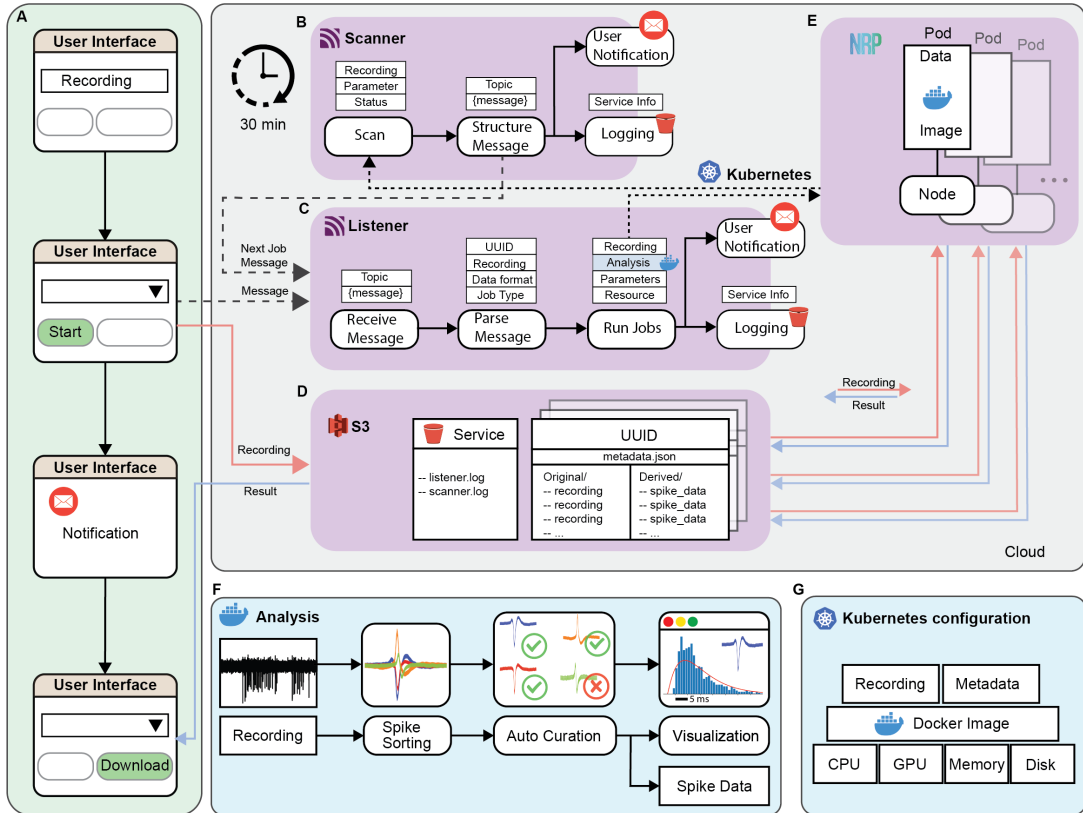


Figure 2: Pipeline components and workflow.. (A) The user interface allows researchers to upload their electrophysiology recordings to cloud storage, initiate data processing jobs, receive notification upon completion, and download results to local computers. (B) MQTT-based job scanner service monitors job status on the NRP, sends a message to the listener for the next job, and notifies users. (C) MQTT-based job listener service that subscribes to specific topics to run data processing jobs. When the service receives a message, it parses the JSON format to extract experiment identifiers and computing requirements, then deploys jobs to NRP through Python-Kubernetes API. Both scanner and listener services update their status to S3 log files on a scheduled basis. (D) S3 file structure for service logging and experiment data. Log files are human-readable text files that track service status. Experiment data is stored in batches, each with a unique identifier (UUID), metadata file, “original” bucket for experiment data, and “derived” bucket for analysis outputs. (E) Computing cluster (NRP) for running containerized jobs using Kubernetes. (F) An analysis container for batch processing is capable of loading electrophysiology recordings, running spike sorting and autocuration algorithms, producing visualization figures, and generating Numpy files for single units. (G) Kubernetes configuration for job deployment to a computing cluster.

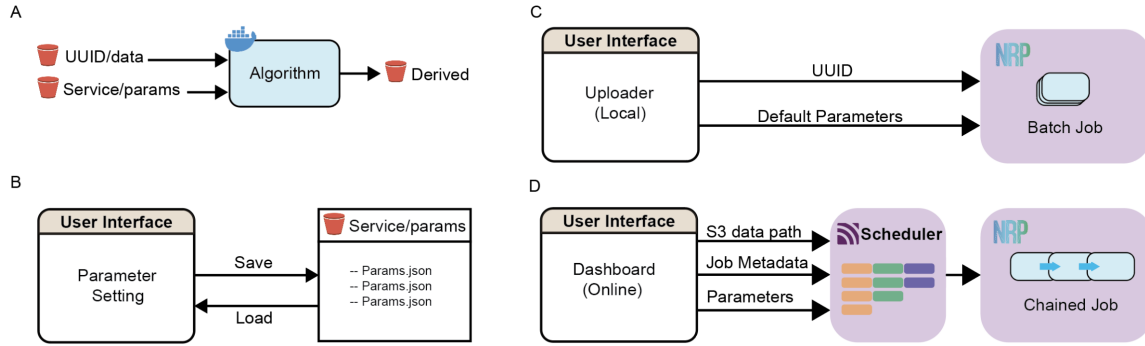


Figure 3: Minimum building block and job types. (A) The minimum pipeline building block utilizing dockerized algorithms and S3 data storage. Data and parameter settings are retrieved from S3, processed by containerized algorithms on NRP, and results are uploaded back to S3. (B) Users can save and load parameter settings to and from the S3 “service” bucket through the Dashboard. (C) Batch processing of numerous recordings is achieved by providing UUID and default parameter settings to the pipeline. Users can initiate this process through the local data uploader. (D) Chained jobs are implemented using a CSV job scheduler containing S3 data paths, job metadata, and parameter settings. Users can initiate job chaining from the online Dashboard.

206 Pipeline Output for Individual Recordings

207 The pipeline output is designed to be comprehensive, structured, and accessible so the data can
208 be reproduced and distributed easily. Using batch processing algorithms, for example, each pro-
209 cessing step produces one compressed file (zip format). For spike sorting, the compressed file
210 is compatible with Phy GUI⁵⁷. Users can download the file, uncompress it, and open it in Phy to
211 check the sorting result and perform manual curation. We also developed a function to load the
212 data directly into a Python object, enabling automated downstream analysis of the single-unit
213 features. Autocuration, the second step, outputs a compressed file (zip format) containing a spike
214 data object in NumPy array and Python dictionary. This object consists of a spike train list, a neu-
215 ron data dictionary, the recording’s sample rate, and electrode configuration. The neuron data
216 dictionary has spatial information such as the channel’s coordinates, neighbor channels, and
217 spike features such as waveform and amplitude. The spike train list and the neuron data dictio-
218 nary index match each other. The size of the autocuration file is approximately 10 times smaller
219 than the spike sorting output by re-constructing the data. For the final step, data visualization, the
220 pipeline generates interactive HTML format figures for the recording and a PNG format figure for
221 each single unit. All of the output files have a log to keep track of the actions and decisions made
222 by the algorithm. To make the data structure consistent, other algorithms’ outputs that are pro-
223 duced by this pipeline are also sorted into NumPy arrays and dictionaries. These outputs can be
224 easily converted to Pandas DataFrame and distributed as tabular data.

225 Figure 4 illustrates the visualization output for a 10-minute recording from a mouse cortical organoid
226 on day 42 in culture. Figure 4A is a photograph of the mouse cortical organoid on the HD-MEA.
227 Initially, two organoids were plated on the same HD-MEA for this experiment. As the majority
228 of activity originated from the right organoid, our analysis was focused on this organoid. The
229 pipeline’s interactive HTML overview figure includes a footprint map showing the spiking wave-
230 forms on the corresponding electrode locations (Figure 4B). The HD-MEA can detect a unit’s
231 footprint by multiple electrodes and potentially show the neuron’s orientation. Since a single elec-
232 trode can record activity from many neurons, different colors are used to label the units. Along-

233 side every single unit's colored footprint (Figure 4B) we provide descriptive electrophysiology
234 features (Figure 4C). We present the unit's temporal firing rate using 50 ms binning of the spike
235 times over the course of the recording (Figure 4C-i). The result is smoothed by a Gaussian ker-
236 nel with a sigma of 5. We also provide the amplitude of each spike and a histogram of the am-
237 plitude distribution (Figure 4C-ii,iv). Raw spikes and the averaged waveform are also displayed
238 (Figure 4C-iii). Both the amplitudes and raw spikes are from the best channel which recorded the
239 highest mean amplitude of the unit. Interspike interval (ISI) is a crucial feature for neurons, as it
240 is associated with firing patterns and cell types^{23,24,58,59}. We show this information through an
241 auto-correlogram in the range of -50 to 50 ms and a histogram of ISI values in the range of 0 to
242 50ms (Figure 4C-v,C-vi).

243 In addition to the footprint map, the interactive HTML overview figure includes a spike raster and
244 several statistical plots for population features for the organoid. The spike raster shows each
245 unit's spike times and the population firing rate with labeled burst peaks (Figure 4D,E). Bursts
246 are detected by thresholding the population firing rate. We show burst features such as the distri-
247 butions of peak firing rate, interburst interval, and each unit's burstiness index in violin plots (Fig-
248 ure 4G). Furthermore, we display the distribution of firing rates, minimum ISI values, and mean
249 spike amplitudes for all single units in the recording (Figure 4F-i,ii,iii). We also illustrate the pair-
250 wise correlation of units' firing activity by calculating the Spike Time Tiling Coefficient (STTC)⁶⁰
251 value of each unit relative to the others. We designed the overview figures to be interactive, al-
252 lowing users to zoom in for a closer examination of the data. The figures for individual units are
253 high-resolution. These figures can give users useful information to evaluate the recording object
254 and perform cross-comparisons. Detailed descriptions of data visualization can be found in the
255 Methods section. The complete figures are available in the Supplementary Figure S4, S5.

256 **Longitudinal Organoid Electrophysiology Properties**

257 Longitudinal neuronal recordings provide invaluable data to study how neuron activity patterns
258 change over time. The cortical organoid shown in Figure 4A was subjected to hourly ten minute
259 recordings on the HD-MEA over seven days (see Voitiuk et al., 2024⁵⁰). During this experiment,
260 recordings were automatically scheduled at the beginning of each hour, uploaded to S3, and pro-
261 cessed by the pipeline. Data processing included spike sorting using Kilosort2 and autocuration
262 with quality metrics. Detailed descriptions of the data processing can be found in the Methods
263 section.

264 Over time, we observed an increasing number of single units and intensified spiking activity. Fig-
265 ure 5A illustrates the time-lapse images of the units' locations and their action potential ampli-
266 tudes on the HD-MEA. With a grayscale color bar, the darker color denotes a higher amplitude.
267 The scale ranges from 0 μ V (white) to 30 μ V (black). There is a noticeable increase in the activity
268 intensity and clustering of active areas as days progress, especially prominent between days 3 to
269 5. To visualize the development of the organoid neuronal network we plotted the number of de-
270 tectable units in each recording (Figure 5C,D) and the individual unit firing rate (Figure 5E,F) over
271 the recording time course. Figure 5C shows the distribution of the unit count across recordings
272 for each day, while figure 5D shows the average number of units each day. There is a substantial
273 growth in the number of units from day 0 to day 2 and decreased variability among the record-
274 ings. From day 2 to day 7, the number of units is relatively stable, with an increased variability
275 across the samples. There is a clear upward trend for the firing rate for the individual neural units
276 from each recording (Figure 5E) and the average firing rate for each day (Figure 5F). As the days
277 progress, the firing rate distribution of individual units becomes wider with some units showing
278 higher firing rates while other units have a firing rate between 0 and 10 Hz.

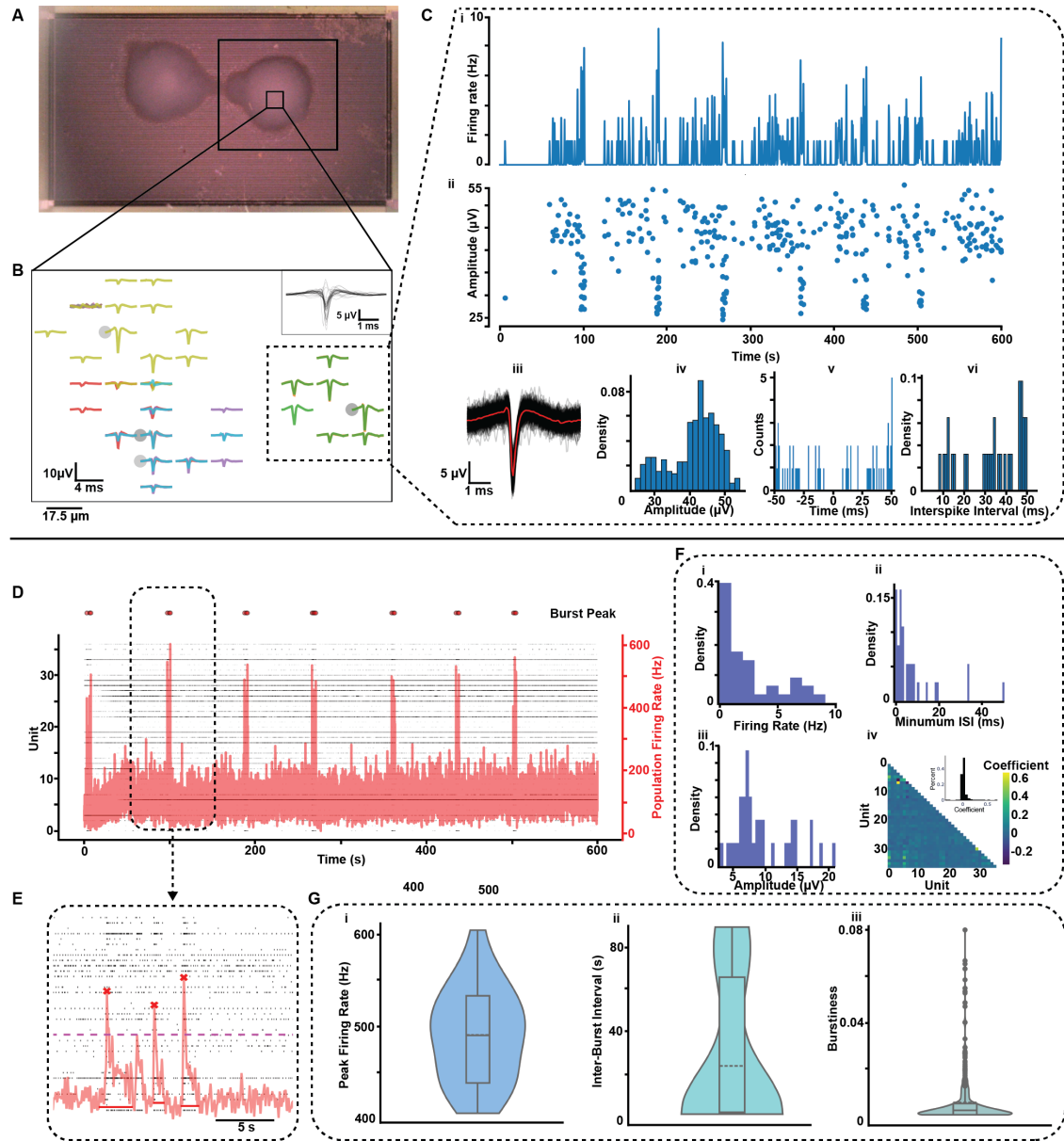


Figure 4: Pipeline Output for an Electrophysiology Recording. (A) Photograph of a mouse organoid on HD-MEA. (B) Zoomed-in view of spiking activities in the mouse organoid. Each color represents a single unit. Waveforms from all single units are shown in the top right corner. (C) Spiking features for the single unit labeled in B: i) Firing rate distribution over the recording time, calculated by binning spike train with a 50 ms time window. ii) Amplitude of each spike over the recording time. iii) Raw spike waveforms (black) and the averaged waveform (red). iv) Amplitude distribution. v) Auto-correlogram from -50 ms to 50 ms. vi) Interspike interval distribution for intervals in the 0 - 50 ms range. (D) Spike raster (black) overlaid with population firing rate (red) for the recording. Dots above the plot label population burst peaks. (E) Zoomed-in view of a population burst. (F) Distribution of i) unit firing rates, ii) minimum ISIs, iii) mean amplitudes, and iv) spike time tiling coefficients. (G) Violin plots showing the distribution of i) population burst peak firing rates, ii) interburst intervals, and iii) burstiness of each single unit.

279 We also found changes in neuron firing patterns over time. The neural unit firing patterns are
280 represented by the coefficient of variation (CV) of interspike intervals (ISI)⁶¹⁶². We show the
281 evolution of CV by plotting the standard deviation of ISI to the mean of ISI for each unit over the
282 7 days. The stacked bar charts represent the proportion of neurons with different CV values,
283 where the red portion indicates neurons with $CV < 1$, and the blue portion represents neurons
284 with $CV \geq 1$ (Figure 5B). Over the 7 days, we observe a trend of an increasing number of units
285 showing a more regular pattern with $CV < 1$, implying the maturity of the neural network. Day 0
286 to day 2 starts with a fairly even split, with slightly more neurons having $CV \geq 1$ (44%, 54%, and
287 53%) and $CV < 1$ (56%, 46%, and 47%). As time progresses, there is a clear shift towards neu-
288 rons with $CV < 1$. By day 6, the majority of neurons have $CV < 1$ (72%), and a small proportion of
289 neurons have $CV \geq 1$ (28%).

290 Overall, this analysis suggests maturation of the mouse cortical organoid neuronal activity over
291 the 7 days with increases in both the number of units detected and their firing rate. The increased
292 firing rate variability could indicate the emergence of more complex and heterogeneous neural
293 circuits within the organoid.

294 **Neuron Tracking for Longitudinal Recordings**

295 The consistency of the pipeline enables tracking putative neurons throughout the longitudinal ex-
296 periment, as the same processing steps and parameters are applied to all datasets. A trackable
297 unit can be identified by its consistent spike waveform and location on the HD-MEA. After spike
298 sorting a recording, we gathered the average waveform (2.5ms), the best channel's location (x,
299 y coordinate on the HD-MEA), footprint, and firing rate for each single unit. We used a waveform
300 clustering algorithm (WaveMap)⁴²⁴ to label the units and observed the change of electrophysi-
301 ological features across multiple days. We ran WaveMap using both the waveform and the best
302 channel's location. The best channel is defined as the one that recorded the unit's highest mean
303 amplitude. For each unit, we concatenated the best channel's location to the end of the wave-
304 form. Then, we aggregated units from all recordings. The waveforms and the locations were nor-
305 malized separately. As a result, WaveMap yielded 20 distinct clusters for the mouse organoid,
306 as shown in Figure 6A. For each cluster, we characterized the waveform features by measuring
307 the trough-to-peak width and Full Width at Half Maximum (FWHM) of the amplitude. The violin
308 plots (Figure 6C) show significant differences in the waveform features among clusters, indicat-
309 ing potentially different cell types in the organoid. Details of running the algorithm can be found in
310 Methods: Waveform Clustering for Cell Tracking.

311 For a trackable unit at a static location on the organoid, the unit's waveforms sampled across
312 recordings should be in the same cluster and appear on adjacent recording channels. Using
313 HD-MEA, we can locate a unit within a small area with an electrode pitch of tens of microme-
314 ters (17.5 μ m for MaxOne HD-MEA). We labeled each footprint by the color of the correspond-
315 ing waveform cluster and observed the duration and change of its best channel throughout the
316 recordings. For each cluster, we summarized the best channels for each recording and the fre-
317 quency of each channel (Supplementary Figure S7) that shows activity.

318 Among these clusters, we selected Cluster 4 as our primary focus (Figure 6B, D). Figure 6B
319 shows this cluster on the UMAP and the waveforms across recordings. We observed the channel
320 locations of the units in this cluster and arranged the footprints from the three adjacent channels
321 that showed the most activity. These activities are highly likely to be from an individual neuron.
322 We labeled the best channels as L1, L2, and L3 and overlaid corresponding footprints for each
323 channel (Figure 6D,E). On an HD-MEA, the electrical signal from a neuron can be picked up by
324 nearby electrodes, which can be beneficial in identifying a neuron's orientation and movement.

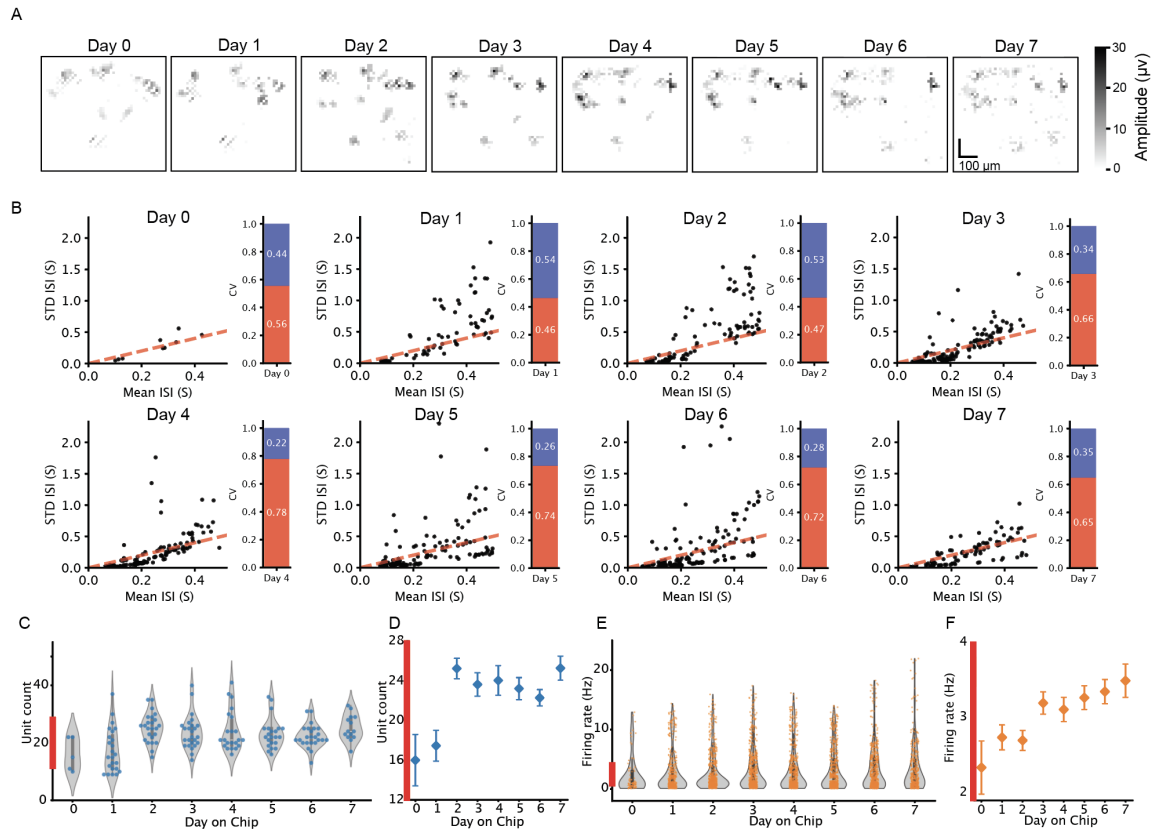


Figure 5: Single neuron features from hourly recordings over days. (A) Spatial area of spiking activity in the mouse organoid on the HD-MEA over the recording time course. Color intensity corresponds to the amplitude of the neuron's action potential. (B) Changes in the Coefficient of Variation (CV) of interspike interval distribution over time. The bar plot shows the percentage of units with $CV < 1$ (red) and $CV \geq 1$ (blue). (C) Distribution of the total number of single units for each day. (D) Average unit count with standard error of the mean (SEM) over time (Day 0: 16 ± 2.58 , Day 1: 17.45 ± 1.55 , Day 2: 25.25 ± 1.03 , Day 3: 23.64 ± 1.18 , Day 4: 24.04 ± 1.49 , Day 5: 23.22 ± 1.12 , Day 6: 22.29 ± 0.81 , Day 7: 25.28 ± 1.20). (E) Single unit firing rate distribution over the 7 days. (F) Average firing rate (Hz) with SEM over time (Day 0: 2.33 ± 0.35 , Day 1: 2.74 ± 0.16 , Day 2: 2.7 ± 0.13 , Day 3: 3.19 ± 0.14 , Day 4: 3.11 ± 0.16 , Day 5: 3.27 ± 0.15 , Day 6: 3.35 ± 0.16 , Day 7: 3.49 ± 0.22)

325 During the experiment, this unit initially showed activity on L3. Then its signals were sampled
326 mostly between the two main locations L1 and L2 (Figure 6F). We calculated the firing rate for
327 each sample across recordings and locations (Figure 6F), and grouped the firing rates for each
328 location in Figure 6G. Interestingly, while distributions of firing rates between L1 and L2 did not
329 differ significantly (two-sample Kolmogorov–Smirnov test, $p=0.11$), there was a significant dif-
330 ference between L2 and L3 distributions (two-sample Kolmogorov–Smirnov test, $p=0.019$). This
331 finding suggests that L3 may represent a subset of activity of L2 based on differences in their re-
332 spective footprints.

333 Using this study, we show the pipeline provides stable, consistent and reproducible data analysis.
334 The neuron tracking function can improve our understanding of an individual neuron's long-term
335 activity by monitoring its electrophysiological features. Thus, this pipeline offers new possibilities
336 to investigate neural dynamics, plasticity, and neural circuit development.

337 **Pipeline Applied to Optogenetics Modulation of Epileptiform Activity from Human Hippocam- 338 pus Slices**

339 Epilepsy is a neurological disorder characterized by abnormal brain activity resulting from an im-
340 balance between excitatory and inhibitory processes⁶³. Light-responsive channelrhodopsins en-
341 able optogenetic interventions to modulate the neuronal activity of brain tissues. We applied this
342 pipeline's data processing and analysis functionality to study the optogenetic modulation of neu-
343 ral circuits from human hippocampus slices.

344 Before optogenetics illumination, human organotypic tissue slices from hippocampus tissue were
345 established. The hippocampus tissue was obtained from patients with drug-refractory tempo-
346 ral lobe epilepsy, sliced to 300 μ m, and cultured at an air-liquid interface. Slices were transduced
347 with AAV9 carrying an HcKCR1 transgene driven by a CaMKII α promoter and a fluorescent tag
348 (eYFP) (see Andrews et al., 2024⁶⁴). A hippocampus slice was plated on an HD-MEA (Max-
349 One) for electrophysiology recording, with a fiber-coupled LED to illuminate the slice from the
350 top. Since HcKCR1 encodes a kalium channelrhodopsin, a light-gated potassium channel that
351 hyperpolarizes the neuronal membrane, the probability of neuronal spiking is reduced when ac-
352 tivated by 530nm light. Bicuculline was applied to the slice after plating to increase neuron firing
353 rates, inducing epileptiform activity. During the experiment, we illuminated the slice for 10 sec-
354 onds at 0.6 light intensity (35.8 mW/mm²) of the LED driver, and observed the neuronal popula-
355 tion firing activity for 10s prior to illumination (Pre-Stim), 10s during illumination (Light-On) and
356 10s following the end of illumination (Light-OFF). The experimental setup is shown in Figure 7A.
357 Each HD-MEA recording was processed by the described pipeline using spike sorting and au-
358 tocuration algorithms. Neuronal activities were aligned to optogenetics stimulation timestamps
359 that were synchronized with the recording. As illustrated in Figure 7B, the units' footprints were
360 overlaid with NeuN staining of the slice on the HD-MEA recording area, showing the physical lo-
361 cation of the spiking activity. Examples of spike waveforms and auto-correlograms are shown.

362 The optogenetics modulation of population firing is shown in Figure 7D and Supplementary Fig-
363 ure S8. The bicuculline-provoked recurrent burst activity was rapidly suppressed by the illumi-
364 nation. Interestingly, the burst activity didn't completely recover when the illumination was off.
365 The firing rate suppression of individual neuronal units was consistent among trials (Figure 7E).
366 This pipeline is capable of providing multiple perspectives of an individual neuron's firing activity
367 (Figure 7C). In addition to firing rate, the suppression of activity is visualized on the hippocam-
368 pus slice through the electrodes on the HD-MEA. The pipeline can extract local field potential
369 (LFP) data by applying a 5th-order Butterworth bandpass (0.1-100Hz) filter to the raw voltage
370 data. During the 10 seconds "Light-ON" period, activities in the LFP frequency bands were also

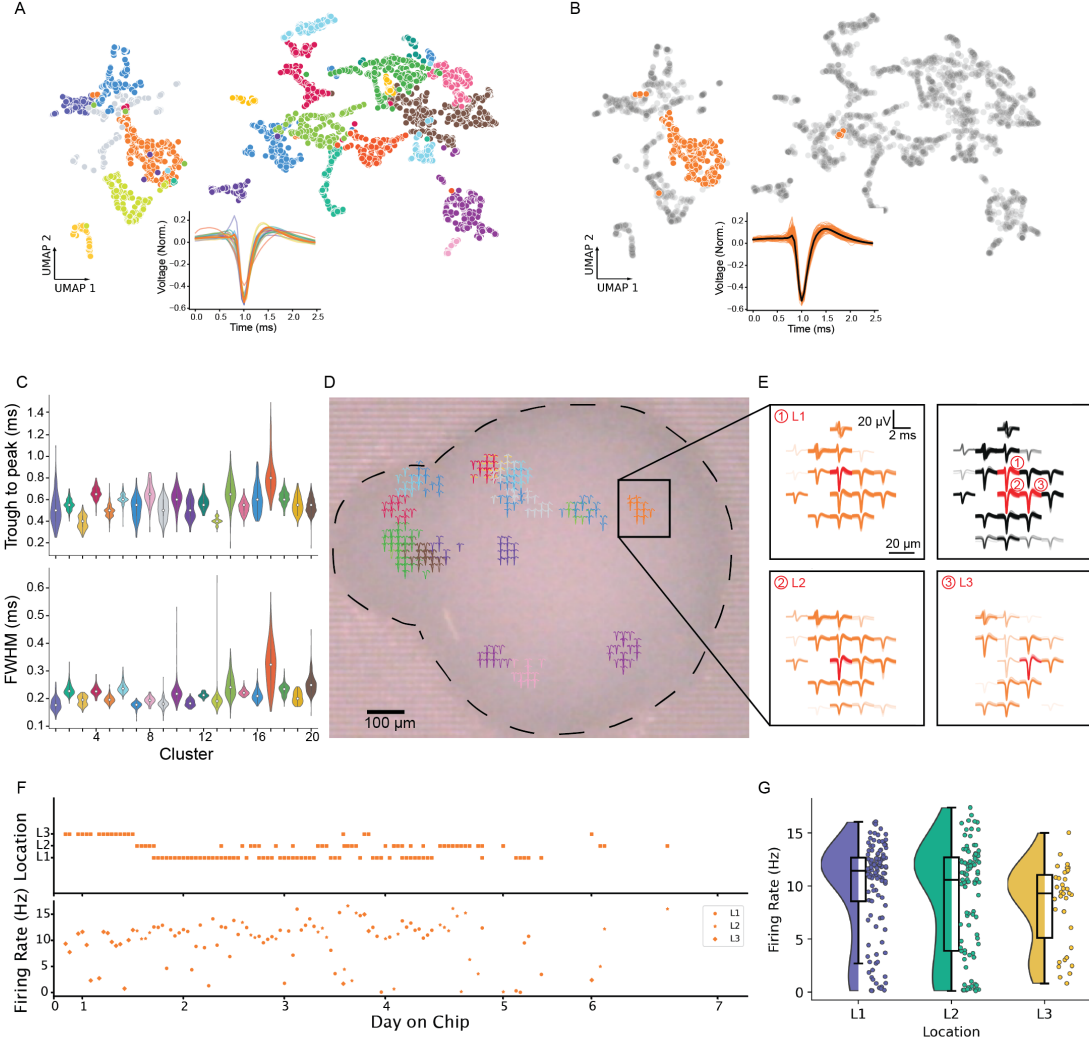


Figure 6: Neuron tracking in a mouse organoid over seven days of recording Pipeline output demonstrating the capability of neuron tracking for longitudinal recordings. (A) UMAP of waveform clusters with location coordinates. The inset shows the mean waveforms of each cluster from a total of 20 clusters superimposed. (B) The cluster of interest (orange) is highlighted on the UMAP, with other clusters in gray. Inset displays the individual waveforms from this cluster, with the mean waveform in black obtained by averaging all the waveforms. (C) Distribution of waveform features for each cluster. The features include trough-to-peak width and Full Width Half Maximum (FWHM) of the amplitude. (D) Footprint projection on the organoid recorded on the MEA. The footprint is color-coded according to the UMAP cluster. (E) Footprints for the cluster of interest overlaid across the recording time course. L1, L2 and L3 are the best channels on the footprints. (F) Temporal tracking of location and firing rate change for the units in the orange cluster. (G) Firing rate distribution for the three locations.

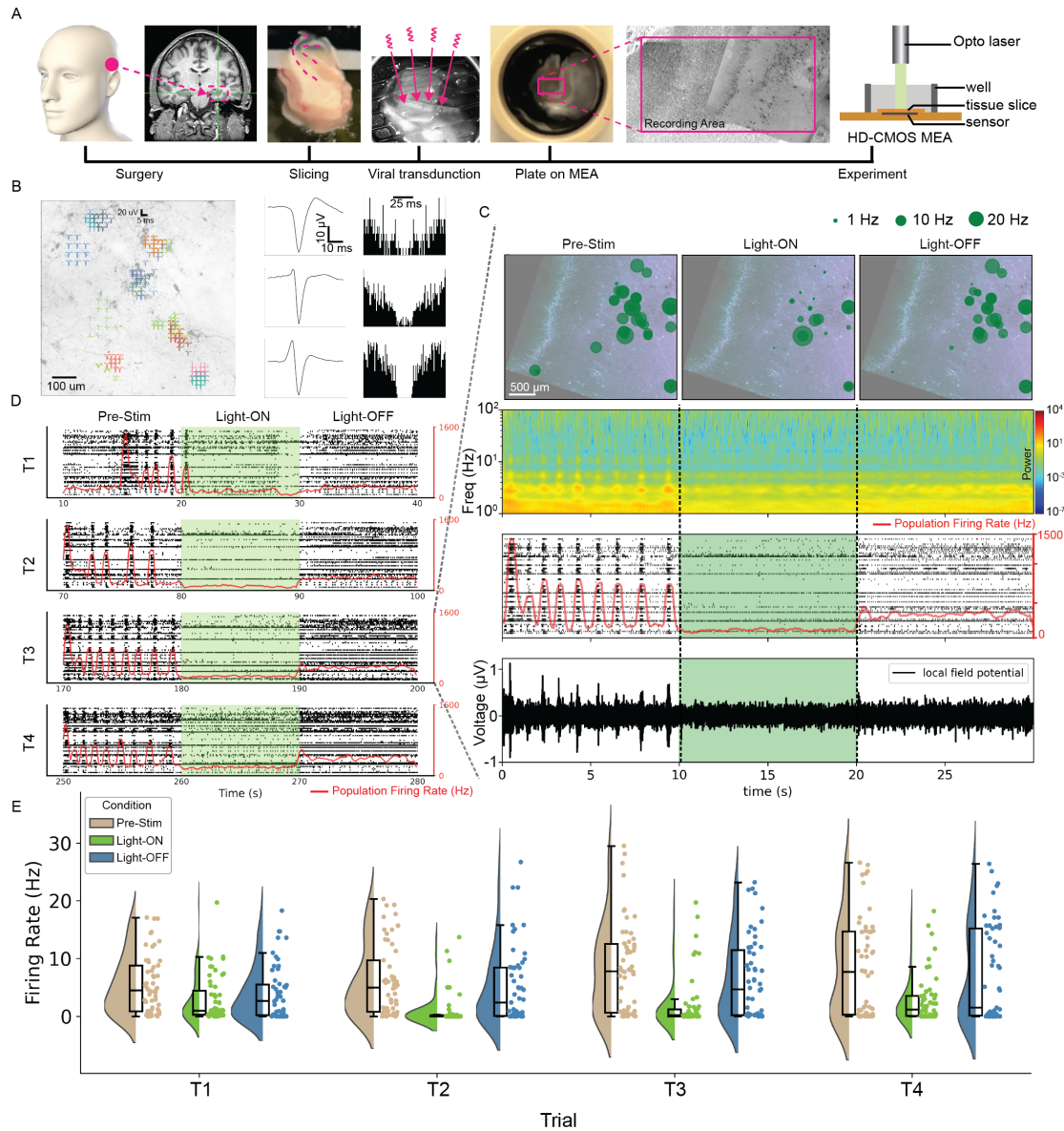


Figure 7: Pipeline facilitates seizure study by analyzing electrophysiology data from human hippocampus brain slice with optogenetic stimulation. (A) Experimental setup for hippocampus slice HD-MEA recording^[64]. Brain tissue from a seizure patient in 300 μm thick slices cultured expressed channelrhodopsin delivered through adeno-associated virus (AAV) delivery. The slice is placed on HD-MEA for simultaneous optogenetic stimulation and recording detailed in Andrews et al., 2024^[64]. (B) NeuN-stained hippocampus slice overlaid with an image of the slice on HD-MEA and footprint of spiking activities on the slice. Example spike waveforms and auto-correlograms from representative neurons. (C) Hippocampus slice overlaid with single units' firing on the HD-MEA. The change in firing activity is shown for the three steps of Trial 3 (T3). From top to bottom, the panels display the single unit's location overlaid with GFP-stained slice, firing rate, local field potential spectrum, spike raster, and voltage data from all recording channels. (D) Spike raster with population firing rate for four experimental trials under Pre-Stim, Light-On, and Light-Off conditions. The population firing rate shows epileptiform activity suppressed by optogenetics illumination, with the firing rate remaining low afterwards. (E) The single unit's firing rate distribution for each Trial in (D).

371 attenuated.

372 This application showcases the pipeline's adaptability to diverse experimental paradigms, ex-
373 tending its utility beyond basic neural activity analysis to more complex neurological disease
374 studies. This advancement opens new avenues for studying neurological disease mechanisms
375 and potentially developing therapeutic approaches, highlighting the pipeline's significance in
376 translational neuroscience research.

377 **DISCUSSION**

378 The cloud-based electrophysiology data pipeline presented in this study represents an advance-
379 ment in the processing and analysis of HD-MEA recordings, which are enabled by IoT and cloud
380 computing technology. The flexible and modular architecture can meet different data processing
381 goals, enabling high data quality and comprehensive electrophysiology feature extraction. The
382 integration of the MQTT messaging protocol provides remote access to the pipeline as well as
383 communications between various components of the pipeline. The cloud-based infrastructure
384 addresses the challenge of storing and processing large volumes of long-term, high-throughput
385 experiments. The parallelized processing capabilities allow for rapid analysis of multiple datasets
386 simultaneously. In addition, the ability to process recordings consistently and without human in-
387 tervention saves time and reduces the potential for human error and bias in data analysis.

388 The user interface allows easy access to the pipeline, and open source makes the pipeline adapt-
389 able to different computing environments and infrastructure setups. Cloud data storage and com-
390 puting contribute to the scalability of the pipeline. The pipeline output data structure is straightfor-
391 ward and size efficient, making it easy for computational tasks.

392 **Consistent and Reliable Data Processing**

393 By using the same parameter settings for spike sorting and curation across all recordings, we en-
394 sure that data is processed uniformly without human intervention. This consistency is crucial for
395 longitudinal studies, where tracking changes in neural activity over time requires a stable and re-
396 producible processing framework. The use of Kilosort2 for spike sorting, combined with autocu-
397 ration algorithms, allows us to accurately identify and classify single-unit activity, even in complex
398 datasets with overlapping spikes. Recent studies have highlighted the importance of such con-
399 sistent processing in large-scale electrophysiology data analysis.

400 One of the most critical aspects of our pipeline is its ability to process data consistently and reli-
401 ably. By using the same parameter settings for spike sorting and curation across all recordings,
402 we ensure that data is processed uniformly without human intervention. This consistency is cru-
403 cial for longitudinal studies, where tracking changes in neural activity over time requires a stable
404 and reproducible processing framework. The use of Kilosort2 for spike sorting, combined with
405 auto-curation algorithms, allows us to accurately identify and classify single-unit activity, even in
406 complex datasets with overlapping spikes. Recent studies have highlighted the importance of
407 such consistent processing in large-scale electrophysiology data analysis³⁰⁻⁶⁵.

408 **Data Management and Visualization**

409 Our pipeline's data management capabilities are enhanced by the use of a hierarchical structure
410 with strategically named buckets on AWS S3. This structure, combined with metadata files that
411 store detailed experiment-related information, ensures that data is organized efficiently and can
412 be accessed quickly. The integration of user interfaces, such as the data uploader and Dash-
413 board, further empowers researchers by providing tools for data management, algorithm param-
414 eter configuration, and result visualization. The Dashboard, built using the Plotly Dash library,

415 offers interactive features that allow users to explore and analyze their data in depth. Similar ap-
416 proaches have been successfully implemented in recent neuroscience data management and
417 visualization systems⁶⁶.

418 **Code Availability**

419 This electrophysiology data pipeline is an open-source project. The code will be released on
420 GitHub upon manuscript publication and is currently available upon request.

421 **Data Availability**

422 No new data was generated for this paper. All datasets described were obtained from Voitiuk et
423 al., 2024⁵⁰, Andrews et al., 2024⁶⁴.

424 **METHODS AND MATERIALS**

425 **Mouse Cortical Organoids**

426 The data presented in this manuscript was collected using an integrated system for neuronal cell
427 culture⁵⁰. Mouse cortical organoids were made using a protocol described in Park et al., 2024⁶⁷.
428 Cortical organoid recordings were performed on a MaxWell Biosystems MaxOne CMOS HD-
429 MEA chip. The system captured 10-minute recordings every hour for seven days. The recording
430 configuration remained consistent throughout the experiment. Details can be found in Voitiuk et
431 al., 2024⁵⁰.

432 **User Interfaces, Data uploader, and Dashboard**

433 To give researchers full control over their experimental data, we designed user interfaces that
434 enable data management, data processing, algorithm parameter configuration, and result visual-
435 ization. We developed the data uploader installed on a local computer of the recording device as
436 well as an online Dashboard for remote data access.

437 The data uploader, created using the Python PyQt library, facilitates the uploading of experi-
438 ment recordings from a local laptop to S3. Upon opening this application, users can navigate
439 to a folder where recordings are stored. An initial Universally Unique Identifier (UUID) is gener-
440 ated using the date of the recordings, and users can add more descriptive labels to this UUID.
441 Before uploading, users must generate a metadata file by loading a template and inputting any
442 experiment-related information such as notes, cell lines, media used for culture, and recording
443 features for each dataset. Recording features such as recording length, number of active chan-
444 nels, and data path are automatically populated in the metadata template. When users press the
445 upload button, all recordings in the selected local folder are reorganized according to the S3 file
446 structure and are uploaded to the UUID folder on S3. Users can start the data analysis pipeline
447 after uploading by sending a request to the job listener.

448 The Dashboard was created using the Python Plotly Dash library. This library uses callback func-
449 tions to achieve user-interactive features like dropdown lists, buttons, and tables. We built a multi-
450 page website, with each page serving a different purpose.

451 On the “Data Processing Center” page, users can choose recordings from the S3 dropdown list,
452 select preferred data processing jobs, set parameters, and start NRP jobs. It allows users to per-
453 form batch processing or chained tasks for chosen recordings. Batch processing is the most
454 commonly used case since all parameters and algorithms are usually the same for an experi-
455 ment. Chained tasks are practical for testing parameter and algorithm combinations for new ex-
456 periment setups. Supplementary Figure S3 shows the job center webpage.

457 On the “Status” page, users can monitor the job status of current tasks on the NRP cluster. By
458 using the “Show Status” button, users can check jobs labeled with prefix “edp-”. This function
459 parses the information returned by Kubernetes Python API for all jobs in the namespace. Upon
460 refreshing with the button, the NRP job name, running status, and data summary will be dis-
461 played on the webpage.
462 The “Visualization” page is designed to display figures of post-processed results. Users can se-
463 lect a processed recording from the dropdown menu to display an interactive raster plot and elec-
464 trode map. Clicking a unit on the electrode map highlights its spike times in light red on the raster
465 plot and shows its waveform and interspike interval histogram. This page allows users to eval-
466 uate MEA recordings effectively.

467 **Cloud Data Storage and Organization**

468 Efficient cloud data organization is crucial for optimizing access performance and storage man-
469 agement. In this pipeline, we employ a hierarchical structure with strategically named buckets.
470 We use a UUID that reflects the experiment date and key information. Upon data uploading,
471 the metadata file is automatically generated and uploaded with the raw data. For each UUID,
472 we keep the raw data in “/original/data”, and the processed result files in “/derived/algo”, where
473 “algo” can be “kilosort2”, “connectivity” and others that are named after the specific algorithms.
474 We store logging files on S3 for MQTT services and data analysis jobs. Detailed logs provide
475 a comprehensive record of each pipeline component by capturing essential information. These
476 logs enable researchers to track the progression of data processing, identify potential bottle-
477 necks, and troubleshoot issues effectively. Service logs are generated when the MQTT broker
478 sends or receives a message and updated to the S3 “/service” bucket on a schedule. Logs from
479 the data analysis jobs include processing steps, quantities, and malfunctions. These log files are
480 kept in the algorithm output directory.

481 **Cloud Orchestration**

482 Each analysis algorithm is packaged into a Docker container with the minimum required de-
483 pendencies, enabling parallel processing of a large volume of electrophysiology recordings in a
484 cloud-agnostic environment. This approach simplifies the addition of new analysis algorithms to
485 the pipeline.
486 We use Kubernetes to deploy and monitor data processing jobs on NRP. For each container,
487 based on the input data size and algorithm requirements, we request computing resources from
488 NRP, such as the number of CPUs, GPUs, memory, and storage. Supplementary Table S2 sum-
489 marizes the computing resource requirements for each algorithm on a 10-minute HD-MEA record-
490 ing with 1000 active channels. When a job is deployed to NRP, a pod with a job is created to run
491 the data in a container. To get the status of the pod, we extract metadata from the return of the
492 Kubernetes “list_namespace_pod” function. From the metadata, we provide the status of the job,
493 such as “running” or “succeeded,” and the timestamps for running this job.

494 **MQTT Messaging Application**

495 To enable remote job execution for a large number of recordings, we implemented services us-
496 ing MQTT messaging. This infrastructure has been previously described^{47,50}. All messaging
497 services are hosted on the Braingeneers UCSC Genomics Institute server. We package these
498 services into Docker containers and manage them using Docker Compose.

499 **Job Listener**

500 We designed a centralized MQTT service to parse analysis job run messages. This service sub-
501 scribes to specific topics and responds by running the corresponding Docker container on the

502 given data. We assign the topics “experiments/upload” for batch processing or “services/csv_job”
503 for chained tasks.

504 The message body is designed according to the different topics. For “experiments/upload”, we
505 use the UUID and recording file name from the metadata.json file. The service can assemble the
506 S3 file path for each recording from this information. The computing requirements for running
507 batch processing jobs are written to a look-up table in the listener service.

508 For “services/csv_job”, we first create a CSV file where each row contains the UUID, recording
509 file name, job type, and computing requirements for running the analysis. We name the CSV
510 file using the current timestamp, upload it to the S3 services bucket, and create a message con-
511 taining the path to the CSV file and the indices of the CSV rows. When the listener receives this
512 message, it pulls the information from the CSV file and deploys jobs using the given indices. Ex-
513 amples of the messages are included in Supplementary Materials.

514 **Job Scanner**

515 When running analysis jobs on the NRP, we use the prefix label “edp-” in the job name. We name
516 batch processing and chained jobs differently. For batch processing, we name the job using a
517 prefix and the recording file name. For chained jobs, we name the job using a prefix, the CSV file
518 name, and the index of the CSV row. This naming convention allows us to parse the job name to
519 determine which analysis algorithm is running on which data.

520 The job scanner is designed to scan the “edp-” jobs on a schedule with two main aims. First, it
521 notifies the job listener when the current step in a chained job is finished. This message body
522 contains the keyword “update”. When the listener receives this message, it checks the corre-
523 sponding CSV file to launch any pending jobs related to the current job. The scanner scans NRP
524 every 2 minutes to minimize delays in running chained jobs. Second, it notifies users of their job
525 status via a Slack channel using the messaging bridge service 18. These notifications are sent
526 every 30 minutes.

527 Job information is pulled from NRP using Python-Kubernetes functions. We use the “list_namespaced_pod”
528 function to get all “edp-” jobs. We loop through them, extracting job name, data file name, job
529 type, and timestamps. This information is stored in a Python dictionary and updated when the
530 scanner service scans NRP on schedule.

531 The scanner identifies job status and sends messages to other MQTT services. For batch pro-
532 cessing jobs, the scanner sends a user notification message when the job status is “pending”,
533 “running”, “failed”, or “succeeded”. Since “failed” and “succeeded” jobs are finished, the scanner
534 removes these jobs from NRP and the dictionary after sending the message. For chained jobs,
535 when a job is finished as “succeeded”, in addition to sending a user notification, the scanner also
536 sends an “update” message to the listener to run the next job.

537 **User Notification to a Slack Channel**

538 Both the job listener and scanner can send user notifications. When a run job message is sent to
539 the listener, and the listener successfully deploys jobs to NRP, a notification is sent to the Slack
540 channel with the S3 data path, job type, and “start” status.

541 To make user notifications human-readable and clear, when the scanner sends messages to the
542 Slack channel, it groups the jobs by UUID and lists the recordings in each UUID.

543 **Spike Sorting**

544 Spike sorting is fundamental in analyzing extracellular recordings for assigning action potentials
545 picked up by electrode channels to neurons in an ensemble. For the HD-MEA recordings, Kilo-
546 sort2 was used to sort the raw voltage data into single unit activity. Since HD-MEAs can record

547 one neuron from tens of channels, it is common for spikes from many neurons to overlap in time
548 on a single channel. The template matching and clustering algorithm in Kilosort2 can distinguish
549 spikes between different neurons based on their waveform. Before spike sorting, the raw data
550 is bandpass filtered using an IIR filter with a 300 - 6000 Hz bandwidth. The data type is con-
551 verted to int16 for running Kilosort2. The voltage detection threshold of Kilosort2 is set to 6 RMS
552 over the baseline. Parameter settings for Kilosort2 are shown in Supplementary Table S1. Spike
553 sorting was performed on the NationalResearch Platform computing cluster with an NVIDIA A10
554 GPU. The sorting output is saved to a compressed file (zip format) and uploaded to S3. The out-
555 put file structure is compatible with the software Phy for performing manual curation. An autocu-
556 ration process is built on top of the sorting result.

557 **Autocuration**

558 The autocuration process is applied after spike sorting for each single unit. To assess data qual-
559 ity and retain good units for downstream analysis, we evaluate each unit by calculating the Inter-
560 spike Interval (ISI) violation ratio, Signal-to-Noise ratio (SNR), firing rate, and spike waveform.

561 We use the curation module from SpikeInterface API³⁰ in our Python script. For ISI violation,
562 we apply the Hill method⁶⁸ of false positive errors with an absolute refractory period of 1.5 ms.
563 We set the maximum violation rate to 20%. The SNR is calculated using the spike amplitude of
564 a unit and the baseline voltage, with a minimum SNR threshold of 5 RMS. The unit's firing rate
565 is defined as the total number of firing events divided by the recording length in seconds. In our
566 default autocuration algorithm, this threshold is set to 0.1 Hz.

567 To check the spiking waveform for a unit, we run the WaveformExtractor class across all active
568 channels and take the average of a maximum of 500 spikes. We then find the best channel and
569 a maximum of eight neighboring locations on a 3x3 grid by sorting their waveform amplitudes
570 on each channel from highest to lowest. The best channel is defined as the channel that cap-
571 tures the neuron's highest mean amplitude among all recording channels. Since HD-MEAs can
572 record one neuron across multiple channels simultaneously, we expect the waveform distribution
573 to have an adequate layout. This layout is defined as the unit's footprint. Thus, we save units that
574 show a waveform on the best channel and at least one neighboring channel within a distance of
575 17.5 μ m for further analysis.

576 **Visualization of Electrophysiology Features**

577 For each recording, the pipeline generates an interactive overview figure in HTML format that in-
578 cludes the activity map of the MEA, the neuron's footprint at its physical location on the map, a
579 spike raster with population burst detection⁷, and a summary of electrophysiology features for all
580 single units. The population firing rate is smoothed using moving average (20 ms window size)
581 applied to aggregated spike trains, then further smoothed using a Gaussian kernel with sigma =
582 20. The population burst detection threshold is set to 2 RMS of the population's baseline firing
583 rate. Burst detection is performed using `scipy.signal.find_peaks` with a minimum peak distance of
584 800 ms. Burst edges are defined as points where the firing rate drops by 90% from the peak on
585 both sides. The "burstiness index"⁶⁹ of a single unit is represented by a number from 0 to 1 that
586 measures the synchronization in spiking activity by binning (40 ms bin size) the spike train. Elec-
587 trophysiology features include interspike interval (ISI), minimum ISI, firing rate, amplitude, spike
588 time tiling coefficient (STTC)⁶⁰ and average spike waveforms. Distributions of these features for
589 all single units are provided in the interactive figure. Each single unit is also paired with a PNG
590 format figure showing the unit's footprint, raw and average spike waveform, auto-correlogram
591 (ACG), ISI distribution, instantaneous firing rate and amplitudes. Both the interactive figure and
592 single unit figures are created using the Plotly Python graphing library. Parameters for the visual-

593 ization are adjustable in the source code.

594 **Waveform Clustering for Cell Tracking**

595 Neuronal cell types and their spiking waveforms are known to be correlated. To demonstrate the
596 capability of tracking units in longitudinal recordings, we performed waveform clustering using
597 the WaveMAP Python package⁴²⁴. This package combines non-linear dimensionality reduction
598 (UMAP) with the Louvain clustering method.

599 To prepare the waveforms, we first extracted the spike times for each single unit through spike
600 sorting. Since the spike time represents the peak of each spike, we initially took a 5 ms window
601 of the complete waveform from the best channel, then averaged across up to 500 spikes. Be-
602 fore input into the WaveMAP algorithm, we centered the waveforms at their peak and truncated
603 them to 1 ms before and 1.5 ms after the peak. Units with positive spikes were not included in
604 this clustering due to the high possibility of axonal signals. We extracted waveforms for each
605 recording, stacked them into a NumPy array, and pre-processed them using L2 normalization.
606 The total number of waveforms was 3526 from 160 recordings.

607 Given that the mouse organoid recordings were taken hourly across seven days, and neurons
608 can migrate during development, we appended the corresponding electrode location (x, y) to the
609 end of each waveform for clustering. The location was normalized as a percentage of the maxi-
610 mum x and y coordinates, respectively, to ensure the data range was within [0, 1], comparable to
611 the normalized waveform.

612 The UMAP parameters were set with 20 neighbors and a minimum distance of 0.1, while the
613 Louvain clustering resolution was set to 1.5. As a result, the algorithm identified 20 distinct clus-
614 ters and assigned a color to each. Based on the clustering results, we plotted the footprint of
615 each unit on the electrode map using the assigned color. Throughout the recordings, we were
616 able to track changes in a neuron's location and firing rate.

617 **Local Field Potential**

618 Local field potentials (LFPs) are low frequency signals up to about 500 Hz that are generated by
619 multiple signal processes in a neural population⁷⁰. These signals are traditionally decomposed
620 into frequency domain. In this pipeline, we focused on LFPs in the range of 0.1 to 100 Hz, and
621 subband frequencies as delta (0.5 - 4 Hz), theta (4 - 8 Hz), alpha (8 - 13 Hz), beta (13 - 30 Hz)
622 and gamma (30 - 50 Hz).

623 To get LFPs and subband frequencies, we first bandpass filter the raw voltage signal from all record-
624 ing channels with 0.1-100 Hz 5-order Butterworth filter. Then, these signals are downsampled 1
625 kHz. A second bandpass filter is applied to separate subband frequencies. We use spectrograms
626 to show the signal strength of different subbands. A spectrogram is the time-frequency spectrum
627 of the local field potential signal, based on the power values, over the given time and frequency
628 range. We applied a continuous wavelet transform (CWT) on the local field potentials to obtain
629 wavelet coefficients and corresponding frequencies using the complex Morlet wavelet ('cmor1-1')
630 in PyCWT library. Signal strength is computed as the magnitude squared of the wavelet coeffi-
631 cients and smoothed using a Gaussian filter with sigma of 2.

ACKNOWLEDGMENTS

This work was supported by the Schmidt Futures Foundation SF 857 and the National Human Genome Research Institute under Award number 1RM1HG011543 (D.H., S.R.S and M.T.), the National Institute of Mental Health of the National Institutes of Health under Award Number R01MH120295

(S.R.S.) and 1U24MH132628 (M.A.M.-R. and D.H.), the National Institutes of Health (NIH) under award number K12GM139185 and the Institute for the Biology of Stem Cells (IBSC) at UC Santa Cruz, the National Science Foundation under award number NSF 2034037 (S.R.S and M.T), and NSF 2134955 (M.T., S.R.S and D.H). This work was supported in part by National Science Foundation (NSF) awards CNS-1730158, ACI-1540112, ACI-1541349, OAC-1826967, OAC-2112167, CNS-2100237, CNS-2120019, the University of California Office of the President, and the University of California San Diego's California Institute for Telecommunications and Information Technology/Qualcomm Institute. Thanks to CENIC for the 100Gbps networks. H.E.S. is partially supported by the Graduate Research Fellowship Program of the National Science Foundation. The authors want to give special thanks to Anna Toledo, Lon Blauvelt, Catharina Lindley, the IBSC Cell Culture Facility (RRID:SCR 021353), National Research Platform (NRP), and the UCSC Life Sciences Microscopy Center (RRID:SCR 021135) for valuable resources and assistance.

AUTHOR CONTRIBUTIONS

J.G., K.V., D.F.P., and A.R. conceived the project and established the cloud storage organization, cloud computing, and IoT codebase. J.G. designed the pipeline architecture, built the pipeline components, contributed to data collection, analyzed and interpreted the data, created figures and wrote the manuscript. A.R. developed the data uploader and contributed to MEA recordings and spike sorting. A.S. assisted with data analysis code. J.L.S. provided insights into pipeline design, interpreted the data, and contributed to data visualizations. R.C. contributed to the conceptualization of the cloud-based data architecture. S.H. and H.E.S. cultured and provided mouse cortical organoids for MEA recording. K.V. and S.T.S. designed and conducted mouse cortical organoid experiments, provided data, and interpreted the data. E.F.C. provided human tissue samples. J.P.A. obtained human tissue samples, designed and conducted experiments, provided data, interpreted the data, and performed histology. J.P.A., J.G., K.V., A.R., and M.A.T.E. conducted optogenetics experiments, gathered data, and interpreted the results. T.J.N., M.A.M.-R., D.H., T.S., S.R.S., and M.T. provided mentorship, intellectual consultation, input on experimental design and analytic methods, discussed the results. M.A.M.-R., D.H., S.R.S., and M.T. provided funding for the project. All authors commented, edited, and approved the manuscript.

AUTHOR COMPETING INTERESTS

K.V. and S.T.S. are a co-founders and D.H., S.R.S, M.T. are advisory board members of Open Culture Science, Inc., a company that may be affected by the research reported in the enclosed paper. All other authors declare no competing interests.

REFERENCES

- [1] Marie Engelene J Obien, Andreas Hierlemann, and Urs Frey. Accurate signal-source localization in brain slices by means of high-density microelectrode arrays. *Scientific reports*, 9(1):788, 2019.
- [2] Hasan Ulusan, Roland Diggelmann, Julian Bartram, Chloe Magnan, Sreedhar Kumar, and Andreas Hierlemann. Multi-functional hd-meas platform for high-resolution impedance imaging and electrophysiological recordings of brain slices. In *2023 IEEE BioSensors Conference (BioSensors)*, pages 1–4. IEEE, 2023.
- [3] Hyogeun Shin, Sohyeon Jeong, Ju-Hyun Lee, Woong Sun, Nakwon Choi, and Il-Joo Cho. 3d high-density microelectrode array with optical stimulation and drug delivery for investigating neural circuit dynamics. *Nature communications*, 12(1):492, 2021.

- [4] Jeffrey Abbott, Avik Mukherjee, Wenxuan Wu, Tianyang Ye, Han Sae Jung, Kevin M Cheung, Rona S Gertner, Markus Basan, Donhee Ham, and Hongkun Park. Multi-parametric functional imaging of cell cultures and tissues with a cmos microelectrode array. *Lab on a Chip*, 22(7):1286–1296, 2022.
- [5] Toki Kobayashi, Kenta Shimba, Taiyo Narumi, Takahiro Asahina, Kiyoshi Kotani, and Yasuhiko Jimbo. Revealing single-neuron and network-activity interaction by combining high-density microelectrode array and optogenetics. *Nature Communications*, 15(1):9547, 2024.
- [6] Manuel Schröter, Congwei Wang, Marco Terrigno, Philipp Hornauer, Ziqiang Huang, Ravi Jagasia, and Andreas Hierlemann. Functional imaging of brain organoids using high-density microelectrode arrays. *MRS bulletin*, 47(6):530–544, 2022.
- [7] Tal Sharf, Tjitse Van Der Molen, Stella MK Glasauer, Elmer Guzman, Alessio P Buccino, Gabriel Luna, Zhuowei Cheng, Morgane Audouard, Kamalini G Ranasinghe, Kiwamu Kudo, et al. Functional neuronal circuitry and oscillatory dynamics in human brain organoids. *Nature communications*, 13(1):4403, 2022.
- [8] Alessandro Maccione, Matteo Garofalo, Thierry Nieus, Mariateresa Tedesco, Luca Berdoni, and Sergio Martinoia. Multiscale functional connectivity estimation on low-density neuronal cultures recorded by high-density cmos micro electrode arrays. *Journal of neuroscience methods*, 207(2):161–171, 2012.
- [9] Jens Duru, Joël Kückler, Stephan J Ihle, Csaba Forró, Aeneas Bernardi, Sophie Girardin, Julian Hengsteler, Stephen Wheeler, János Vörös, and Tobias Ruff. Engineered biological neural networks on high density cmos microelectrode arrays. *Frontiers in neuroscience*, 16:829884, 2022.
- [10] Timothy P.H. Sit, Rachael C. Feord, Alexander W.E. Dunn, Jeremi Chabros, David Oluigbo, Hugo H. Smith, Lance Burn, Elise Chang, Alessio Boschi, Yin Yuan, George M. Gibbons, Mahsa Khayat-Khoei, Francesco De Angelis, Erik Hemberg, Martin Hemberg, Madeline A. Lancaster, Andras Lakatos, Stephen J. Eglen, Ole Paulsen, and Susanna B. Mierau. Meanap: A flexible network analysis pipeline for neuronal 2d and 3d organoid multielectrode recordings. *Cell Reports Methods*, page 100901, 2024.
- [11] Ian H Stevenson and Konrad P Kording. How advances in neural recording affect data analysis. *Nature neuroscience*, 14(2):139–142, 2011.
- [12] John P Cunningham and Byron M Yu. Dimensionality reduction for large-scale neural recordings. *Nature neuroscience*, 17(11):1500–1509, 2014.
- [13] Anne E Urai, Brent Doiron, Andrew M Leifer, and Anne K Churchland. Large-scale neural recordings call for new insights to link brain and behavior. *Nature neuroscience*, 25(1):11–19, 2022.
- [14] Kenneth D Harris, Rodrigo Quijan Quiroga, Jeremy Freeman, and Spencer L Smith. Improving data quality in neuronal population recordings. *Nature neuroscience*, 19(9):1165–1174, 2016.
- [15] Liam Paninski and John P Cunningham. Neural data science: accelerating the experiment-analysis-theory cycle in large-scale neuroscience. *Current opinion in neurobiology*, 50:232–241, 2018.
- [16] Cleber A Trujillo, Richard Gao, Priscilla D Negraes, Jing Gu, Justin Buchanan, Sebastian Preissl, Allen Wang, Wei Wu, Gabriel G Haddad, Isaac A Chaim, et al. Complex oscillatory waves emerging from cortical organoids model early human brain network development. *Cell stem cell*, 25(4):558–569, 2019.
- [17] Jeremy Magland, James J Jun, Elizabeth Lovero, Alexander J Morley, Cole Lincoln Hurwitz, Alessio Paolo Buccino, Samuel Garcia, and Alex H Barnett. Spikeforest, reproducible web-facing ground-truth validation of automated neural spike sorters. *Elife*, 9:e55167, 2020.

- [18] Alessio P Buccino, Samuel Garcia, and Pierre Yger. Spike sorting: new trends and challenges of the era of high-density probes. *Progress in Biomedical Engineering*, 4(2):022005, 2022.
- [19] Marius Pachitariu, Nicholas Steinmetz, Shabnam Kadir, Matteo Carandini, and Harris Kenneth D Kilosort. realtime spike-sorting for extracellular electrophysiology with hundreds of channels. *biorxiv. Preprint at*, 2016.
- [20] Pierre Yger, Giulia LB Spampinato, Elric Esposito, Baptiste Lefebvre, Stéphane Deny, Christophe Gardella, Marcel Stimberg, Florian Jetter, Guenther Zeck, Serge Picaud, et al. A spike sorting toolbox for up to thousands of electrodes validated with ground truth recordings in vitro and in vivo. *Elife*, 7:e34518, 2018.
- [21] Gerrit Hilgen, Martino Sorbaro, Sahar Pirmoradian, Jens-Oliver Muthmann, Ibolya Edit Kepiro, Simona Ullo, Cesar Juarez Ramirez, Albert Puente Encinas, Alessandro Maccione, Luca Berdondini, et al. Unsupervised spike sorting for large-scale, high-density multielectrode arrays. *Cell reports*, 18(10):2521–2532, 2017.
- [22] Alessio Paolo Buccino, Xinyue Yuan, Vishalini Emmenegger, Xiaohan Xue, Tobias Gänsswein, and Andreas Hierlemann. An automated method for precise axon reconstruction from recordings of high-density micro-electrode arrays. *Journal of neural engineering*, 19(2):026026, 2022.
- [23] Peter C Petersen, Joshua H Siegle, Nicholas A Steinmetz, Sara Mahallati, and György Buzsáki. Cellexplorer: A framework for visualizing and characterizing single neurons. *Neuron*, 109(22):3594–3608, 2021.
- [24] Eric Kenji Lee, Hymavathy Balasubramanian, Alexandra Tsolias, Stephanie Udochukwu Anakwe, Maria Medalla, Krishna V Shenoy, and Chandramouli Chandrasekaran. Non-linear dimensionality reduction on extracellular waveforms reveals cell type diversity in premotor cortex. *Elife*, 10:e67490, 2021.
- [25] Philipp Hornauer, Gustavo Prack, Nadia Anastasi, Silvia Ronchi, Taehoon Kim, Christian Donner, Michele Fiscella, Karsten Borgwardt, Verdon Taylor, Ravi Jagasia, et al. Deepphys: A machine learning–assisted platform for electrophysiological phenotyping of human neuronal networks. *Stem Cell Reports*, 19(2):285–298, 2024.
- [26] Julian Bartram, Felix Franke, Sreedhar Saseendran Kumar, Alessio Paolo Buccino, Xiaohan Xue, Tobias Gänsswein, Manuel Schröter, Taehoon Kim, Krishna Chaitanya Kasuba, and Andreas Hierlemann. Parallel reconstruction of the excitatory and inhibitory inputs received by single neurons reveals the synaptic basis of recurrent spiking. *bioRxiv*, pages 2023–01, 2023.
- [27] Christian Donner, Julian Bartram, Philipp Hornauer, Taehoon Kim, Damian Roqueiro, Andreas Hierlemann, Guillaume Obozinski, and Manuel Schröter. Ensemble learning and ground-truth validation of synaptic connectivity inferred from spike trains. *PLOS Computational Biology*, 20(4):e1011964, 2024.
- [28] NeuroScope Klusters. Ndmanager: a free software suite for neurophysiological data processing and visualization; I hazan, m zugaro, g buzsáki. *Journal of Neuroscience Methods*, pages 207–216.
- [29] George Dimitriadis, Joana P Neto, and Adam R Kampff. t-sne visualization of large-scale neural recordings. *Neural computation*, 30(7):1750–1774, 2018.
- [30] Alessio P Buccino, Cole L Hurwitz, Samuel Garcia, Jeremy Magland, Joshua H Siegle, Roger Hurwitz, and Matthias H Hennig. Spikeinterface, a unified framework for spike sorting. *Elife*, 9:e61834, 2020.
- [31] G Viejo, D Levenstein, S Skromne Carrasco, D Mehrotra, S Mahallati, GR Vite, H Denny,

L Sjulson, FP Battaglia, and A Peyrache. Pynapple, a toolbox for data analysis in neuroscience. *elife* 12, rp85786, 2023.

[32] Konstantinos Nasiotis, Martin Cousineau, François Tadel, Adrien Peyrache, Richard M Leahy, Christopher C Pack, and Sylvain Baillet. Integrated open-source software for multiscale electrophysiology. *Scientific Data*, 6(1):231, 2019.

[33] Nand Chandravadia, Dehua Liang, Andrea GP Schjetnan, April Carlson, Mailys Faraut, Jeffrey M Chung, Chrystal M Reed, Ben Dichter, Uri Maoz, SK Kalia, et al. A nwb-based dataset and processing pipeline of human single-neuron activity during a declarative memory task. *Scientific Data*, 7(1):78, 2020.

[34] Taiga Abe, Ian Kinsella, Shreya Saxena, E Kelly Buchanan, Joao Couto, John Briggs, Sian Lee Kitt, Ryan Glassman, John Zhou, Liam Paninski, et al. Neuroscience cloud analysis as a service: An open-source platform for scalable, reproducible data analysis. *Neuron*, 110(17):2771–2789, 2022.

[35] Zoltan Juhasz. Quantitative cost comparison of on-premise and cloud infrastructure based eeg data processing. *Cluster Computing*, 24(2):625–641, 2021.

[36] Soichi Hayashi, Bradley A Caron, Anibal Sólón Heinsfeld, Sophia Vinci-Booher, Brent McPherson, Daniel N Bullock, Giulia Bertò, Guiomar Niso, Sandra Hanekamp, Daniel Levitas, et al. brainlife. io: a decentralized and open-source cloud platform to support neuroscience research. *Nature methods*, 21(5):809–813, 2024.

[37] Joost B Wagenaar, Benjamin H Brinkmann, Zachary Ives, Gregory A Worrell, and Brian Litt. A multimodal platform for cloud-based collaborative research. In *2013 6th international IEEE/EMBS conference on neural engineering (NER)*, pages 1386–1389. IEEE, 2013.

[38] Steven Baldassano, Xuelong Zhao, Benjamin Brinkmann, Vaclav Kremen, John Bernabei, Mark Cook, Timothy Denison, Gregory Worrell, and Brian Litt. Cloud computing for seizure detection in implanted neural devices. *Journal of neural engineering*, 16(2):026016, 2019.

[39] Ling-Hong Hung, Evan Straw, Shishir Reddy, Robert Schmitz, Zachary Colburn, and Ka Yee Yeung. Cloud-enabled biodepot workflow builder integrates image processing using fiji with reproducible data analysis using jupyter notebooks. *Scientific Reports*, 12(1):14920, 2022.

[40] Saskia EJ de Vries, Joshua H Siegle, and Christof Koch. Sharing neurophysiology data from the allen brain observatory. *Elife*, 12:e85550, 2023.

[41] Robert Hider Jr, Dean Kleissas, Timothy Gion, Daniel Xenes, Jordan Matelsky, Derek Pryor, Luis Rodriguez, Erik C Johnson, William Gray-Roncal, and Brock Wester. The brain observatory storage service and database (bossdb): a cloud-native approach for petascale neuroscience discovery. *Frontiers in Neuroinformatics*, 16:828787, 2022.

[42] Grant Wallace, Stephen Polcyn, Paula P Brooks, Anne C Mennen, Ke Zhao, Paul S Scotti, Sebastian Michelmann, Kai Li, Nicholas B Turk-Browne, Jonathan D Cohen, et al. Rt-cloud: A cloud-based software framework to simplify and standardize real-time fmri. *NeuroImage*, 257:119295, 2022.

[43] Christopher J Markiewicz, Krzysztof J Gorgolewski, Franklin Feingold, Ross Blair, Yaroslav O Halchenko, Eric Miller, Nell Hardcastle, Joe Wexler, Oscar Esteban, Mathias Goncalves, et al. The openneuro resource for sharing of neuroscience data. *Elife*, 10:e71774, 2021.

[44] Priyanka Subash, Alex Gray, Misque Boswell, Samantha L Cohen, Rachael Garner, Sana Salehi, Calvary Fisher, Samuel Hobel, Satrajit Ghosh, Yaroslav Halchenko, et al. A comparison of neuroelectrophysiology databases. *Scientific Data*, 10(1):719, 2023.

[45] Zahra Nasiri Aghdam, Amir Masoud Rahmani, and Mehdi Hosseinzadeh. The role of the internet of things in healthcare: Future trends and challenges. *Computer methods and programs in biomedicine*, 199:105903, 2021.

- [46] Mohammad Nuruzzaman Bhuiyan, Md Mahbubur Rahman, Md Masum Billah, and Dipanita Saha. Internet of things (iot): A review of its enabling technologies in healthcare applications, standards protocols, security, and market opportunities. *IEEE Internet of Things Journal*, 8(13):10474–10498, 2021.
- [47] David F Parks, Kateryna Voitiuk, Jinghui Geng, Matthew AT Elliott, Matthew G Keefe, Erik A Jung, Ash Robbins, Pierre V Baudin, Victoria T Ly, Nico Hawthorne, et al. Iot cloud laboratory: Internet of things architecture for cellular biology. *Internet of Things*, 20:100618, 2022.
- [48] Pierre V Baudin, Raina E Sacksteder, Atesh K Worthington, Kateryna Voitiuk, Victoria T Ly, Ryan N Hoffman, Matthew AT Elliott, David F Parks, Rebecca Ward, Sebastian Torres-Montoya, et al. Cloud-controlled microscopy enables remote project-based biology education in underserved latinx communities. *Helicon*, 8(11), 2022.
- [49] Kateryna Voitiuk, Jinghui Geng, Matthew G Keefe, David F Parks, Sebastian E Sanso, Nico Hawthorne, Daniel B Freeman, Rob Currie, Mohammed A Mostajo-Radji, Alex A Pollen, et al. Light-weight electrophysiology hardware and software platform for cloud-based neural recording experiments. *Journal of neural engineering*, 18(6):066004, 2021.
- [50] Kateryna Voitiuk, Spencer T Seiler, Mirella Pessoa de Melo, Jinghui Geng, Sebastian Hernandez, Hunter E Schweiger, Jess L Sevetson, David F Parks, Ash Robbins, Sebastian Torres-Montoya, et al. A feedback-driven iot microfluidic, electrophysiology, and imaging platform for brain organoid studies. *bioRxiv*, pages 2024–03, 2024.
- [51] Matthew AT Elliott, Hunter E Schweiger, Ash Robbins, Samira Vera-Choqueccota, Drew Ehrlich, Sebastian Hernandez, Kateryna Voitiuk, Jinghui Geng, Jess L Sevetson, Cordero Core, et al. Internet-connected cortical organoids for project-based stem cell and neuroscience education. *eneuro*, 10(12), 2023.
- [52] Kubernetes. <https://kubernetes.io>.
- [53] Oliver Rübel, Andrew Tritt, Benjamin Dichter, Thomas Braun, Nicholas Cain, Nathan Clack, Thomas J Davidson, Max Dougherty, Jean-Christophe Fillion-Robin, Nile Graddis, et al. Nwb: N 2.0: an accessible data standard for neurophysiology. *BioRxiv*, page 523035, 2019.
- [54] Jeffery L Teeters, Keith Godfrey, Rob Young, Chinh Dang, Claudia Friedsam, Barry Wark, Hiroki Asari, Simon Peron, Nuo Li, Adrien Peyrache, et al. Neurodata without borders: creating a common data format for neurophysiology. *Neuron*, 88(4):629–634, 2015.
- [55] Neurodata without borders: Neurophysiology. <https://www.nwb.org/nwb-neurophysiology/>
- [56] Jan Müller, Marco Ballini, Paolo Livi, Yihui Chen, Milos Radivojevic, Amir Shadmani, Vijay Viswam, Ian L Jones, Michele Fiscella, Roland Diggelmann, et al. High-resolution cmos mea platform to study neurons at subcellular, cellular, and network levels. *Lab on a Chip*, 15(13):2767–2780, 2015.
- [57] phy: Spike sorting and ephys data analysis for 1000 channels and beyond. <https://pypi.org/project/phy/>. Accessed: [Insert access date here].
- [58] A Schneider, M Azabou, L McDougall-Vigier, DF Parks, S Ensley, K Bhaskaran-Nair, T Nowakowski, EL Dyer, and KB Hengen. Transcriptomic cell type structures in vivo neuronal activity across multiple timescales. *cell rep* 42: 112318, 2023.
- [59] Eric Kenji Lee, Asim Gul, Greggory Heller, Anna Lakunina, Santiago Jaramillo, Paweł Przytycki, and Chandramouli Chandrasekaran. Physmap-interpretable in vivo neuronal cell type identification using multi-modal analysis of electrophysiological data. *BioRxiv*, pages 2024–02, 2024.
- [60] Catherine S Cutts and Stephen J Eglen. Detecting pairwise correlations in spike trains: an objective comparison of methods and application to the study of retinal waves. *Journal of Neuroscience*, 34(43):14288–14303, 2014.

- [61] Chris Christodoulou and Guido Bugmann. Coefficient of variation vs. mean interspike interval curves: What do they tell us about the brain? *Neurocomputing*, 38:1141–1149, 2001.
- [62] Martin P Nawrot, Clemens Boucsein, Victor Rodriguez Molina, Alexa Riehle, Ad Aertsen, and Stefan Rotter. Measurement of variability dynamics in cortical spike trains. *Journal of neuroscience methods*, 169(2):374–390, 2008.
- [63] Eline J. H. van Hugte, Dirk Schubert, and Nael Nadif Kasri. Excitatory/inhibitory balance in epilepsies and neurodevelopmental disorders: Depolarizing -aminobutyric acid as a common mechanism. *Epilepsia*, 64(5):1234–1245, 2023.
- [64] John P. Andrews, Jinghui Geng, Kateryna Voitiuk, Matthew A.T. Elliott, David Shin, Ash Robbins, Alex Spaeth, Albert Wang, Lin Li, Daniel Solis, Matthew G. Keefe, Jessica L. Sevetson, Julio Rivera-de Jesus, Kevin C. Donohue, H. Hanh Larson, Drew Ehrlich, Kurtis I. Auguste, Sofie Salama, Vikaas Sohal, Tal Sharf, David Haussler, Cathryn R. Cadwell, David V. Schaffer, Edward F. Chang, Mircea Teodorescu, and Tomasz Jan Nowakowski. Multimodal evaluation of network activity and optogenetic interventions in human hippocampal slices. *Nature Neuroscience*, November 2024.
- [65] Carsen Stringer and Marius Pachitariu. Analysis methods for large-scale neuronal recordings. *Science*, 386(6722):eadp7429, 2024.
- [66] Arjun Mahadevan, Neela K Codadu, and R Ryley Parrish. Xenon lfp analysis platform is a novel graphical user interface for analysis of local field potential from large-scale mea recordings. *Frontiers in Neuroscience*, 16:904931, 2022.
- [67] Yunjeong Park, Sebastian Hernandez, Cristian O Hernandez, Hunter E Schweiger, Houpu Li, Kateryna Voitiuk, Harika Dechiraju, Nico Hawthorne, Elana M Muzzy, John A Selberg, et al. Modulation of neuronal activity in cortical organoids with bioelectronic delivery of ions and neurotransmitters. *Cell Reports Methods*, 4(1), 2024.
- [68] Daniel N Hill, Samar B Mehta, and David Kleinfeld. Quality metrics to accompany spike sorting of extracellular signals. *Journal of Neuroscience*, 31(24):8699–8705, 2011.
- [69] Daniel A Wagenaar, Radhika Madhavan, Jerome Pine, and Steve M Potter. Controlling bursting in cortical cultures with closed-loop multi-electrode stimulation. *Journal of Neuroscience*, 25(3):680–688, 2005.
- [70] Gaute T Einevoll, Christoph Kayser, Nikos K Logothetis, and Stefano Panzeri. Modelling and analysis of local field potentials for studying the function of cortical circuits. *Nature Reviews Neuroscience*, 14(11):770–785, 2013.